

A finite difference scheme for integrating the Takagi-Taupin equations on an arbitrary orthogonal grid

Mads Carlsen¹ and Hugh Simons¹

¹Department of Physics, Technical University of Denmark, 2800 Kgs. Lyngby, Denmark

ABSTRACT

Calculation of dynamical diffraction patterns for X-ray topography and similar x-ray scattering-imaging techniques require the numerical integration of the Takagi-Taupin equations. This is usually done with a simple second order finite difference scheme on a sheared computational grid with two of the axes aligned with the wave vectors of the incident and scattered beams respectively. Here we present a finite difference scheme that carries out this integration on an arbitrary orthogonal grid by implicitly utilizing Fourier interpolation. The scheme achieves the expected second order convergence and a similar error to the traditional approach on similarly dense grids but is more computationally expensive due to the use of FFT operations.

Keywords: Dynamical diffraction, Exponential Runge-Kutta

INTRODUCTION

In an effort to understand the origin of errors and aberrations in dark-field x-ray microscopy, we have been simulating images using wave-optics approaches based on the algorithms given by Li et al. (2020). These methods implicitly use Fourier interpolation to calculate the kinematical x-ray scattering by strained crystals from a representation of the crystal on an orthogonal grid in real-space in contrast to the more natural grid that has its axes aligned with the incident and scattered beams. The use of this orthogonal grid has a number of clear advantages, especially when the calculation of the scattered beam is combined with other numerical methods used to generate the input for the crystal structure and the incident radiation, and when the calculated diffraction patterns are further input into simulations of the down-stream optics.

Typically in DFXM, one tries to avoid dynamical effects by using highly deformed samples, small grains or relying on the "weak beam approximation", measuring at the tails of the rocking curve. In many cases, however, dynamical effects are unavoidable and we need to be able to simulate these as well. We therefore set out to find a method of integrating the dynamical Takagi-Taupin equations on an orthogonal grid, in order to impact the rest of the simulation flow as little as possible.

The most obvious way to do this is to interpolate the values of the crystal scattering function from the orthogonal grid, on which it is known, onto a sheared grid and then integrate the TTEs using established finite difference schemes. In order to avoid interpolation artifacts, which would be highly problematic for the simulation of down-stream optics, we would have to use Fourier interpolation. It is not clear how this extra interpolation step would impact the convergence behaviour of the established methods so rather we looked for a systematic way to include this interpolation in the finite difference scheme itself. In the following we present a way to do this based on exponential Rosenbock methods. The end result is similar to the mixed real-space/reciprocal-space methods called "multistep methods" used to model a wide range of optical problems.

1 DYNAMICAL DIFFRACTION

The most general framework for treating dynamical diffraction from strained crystals is the Takagi-Taupin equations (TTE)[Takagi (1962, 1969); Taupin (1967)] which, in the simplest two-beam case assuming σ polarization and exact satisfaction of the Bragg condition, can be written as:

$$\begin{aligned} 2i\mathbf{k}_0 \cdot \nabla E_0(\mathbf{r}) &= k^2(\chi_0 E_0(\mathbf{r}) + \chi'_h(\mathbf{r})E_h(\mathbf{r})) \\ 2i\mathbf{k}_h \cdot \nabla E_h(\mathbf{r}) &= k^2(\chi_0 E_h(\mathbf{r}) + \chi'_h(\mathbf{r})E_0(\mathbf{r})) \end{aligned} \quad (1)$$

where E_0 and E_h are the complex envelopes of the monochromatic fields of the incident and scattered beams respectively. \mathbf{k}_0 is the wave vector of the incident wave in vacuum and $\mathbf{k}_h = \mathbf{k}_0 + \mathbf{Q}$ is the wave-vector of the scattered beam. The choice of \mathbf{k}_0 when writing up the TTEs is arbitrary and leads to different versions of the TTEs. This particular choice gives what is called the symmetric TTEs in the literature.

χ_h and χ'_h are the spatially varying Fourier components of the electric susceptibility corresponding to the Bragg reflection with scattering vector \mathbf{Q} and $-\mathbf{Q}$ respectively. They are related to the Fourier components of the perfect lattice of the undeformed crystal, χ_h and $\chi_{\bar{h}}$ through:

$$\begin{aligned} \chi'_h(\mathbf{r}) &= \exp(i\mathbf{Q} \cdot \mathbf{u}(\mathbf{r}))\chi_h \\ \chi'_{\bar{h}}(\mathbf{r}) &= \exp(-i\mathbf{Q} \cdot \mathbf{u}(\mathbf{r}))\chi_{\bar{h}} \end{aligned} \quad (2)$$

where $\mathbf{u}(\mathbf{r})$ is the displacement field of the crystal. These constants are the macroscopic equivalents of the more often used formfactors and are related to these through:

$$\chi_h = -\left(\frac{4\pi r_0}{k^2 V_{u.c.}}\right)F_h \quad (3)$$

If we ignore the scattering terms, the equations (1) are a pair of convection equations and the solution involves the interpolation of the initial condition through the integration volume. Direct application of a finite-difference scheme in a Cartesian coordinate system would lead to interpolation errors accumulating at each step giving an unwanted dispersion of the initial condition. The traditional approach is therefore to solve the equation in an oblique coordinate system with the axes aligned with the incident and scattered wave-vectors.

The TTEs have been solved by finite difference integration on a structured grid of constant [Authier et al. (1968)] or varying step-sizes[Epelboin (1981)] or by an iterative approach.[Bremer (1984); Yan and Li (2014)] For certain symmetric geometries the sheared coordinate system coincides with a rectangular one.[Kolosov and Punegov (2005); Osterhoff (2012)] Recent efforts have also been made to calculate dynamical diffraction patterns from unstructured grids using a finite element approach. [Honkanen et al. (2018)]

2 DERIVATION

We want to numerically integrate the Takagi-Taupin equations on an orthogonal grid with the three unit-vectors $\hat{\mathbf{x}}$, $\hat{\mathbf{y}}$, and $\hat{\mathbf{z}}$. The only restriction on the choice of coordinate system is that:

$$\mathbf{k}_0 \cdot \hat{\mathbf{z}} > 0 \quad \text{and} \quad \mathbf{k}_h \cdot \hat{\mathbf{z}} > 0 \quad (4)$$

So that the z-axis takes the role of a quasi-optical axis. We introduce the notation $\mathbf{k}_0 = k_{0,z}\hat{\mathbf{z}} + \mathbf{k}_{0,\perp}$ and similar for \mathbf{k}_h and re-write the TTEs as:

$$2k_{0,z}\frac{\partial}{\partial z}E_0(\mathbf{r}) = -ik^2\chi_0 E_0(\mathbf{r}) - 2(\mathbf{k}_{0,\perp} \cdot \nabla_{\perp})E_0(\mathbf{r}) - ik^2\chi'_h(\mathbf{r})E_0(\mathbf{r}) \quad (5)$$

The equivalent equation for E_h is found by substituting subscripts. We define the transverse-Fourier transform:

$$\mathcal{F}_\perp\{E(x,y,z)\}(q_x,q_y,z) = \int \int E(x,y,z) \exp(-i2\pi(xq_x + yq_y)) dx dy \quad (6)$$

With this definition, we Fourier-transform the preceding equation:

$$\frac{\partial}{\partial z} \tilde{E}_0(q_x, q_y, z) = \left[\frac{-ik^2}{2k_{0,z}} \chi_0 - \frac{i2\pi}{k_{0,z}} \mathbf{q} \cdot \mathbf{k}_{0,\perp} \right] \tilde{E}_0(q_x, q_y, z) - \frac{ik^2}{2k_{0,z}} F_\perp \{ \chi'_h(x,y,z) E_h(x,y,z) \} \quad (7)$$

We introduce the angles, α_0 and α_h given by $\mathbf{k}_0 \cdot \hat{\mathbf{z}} = |\mathbf{k}_0| \cos(\alpha_0)$ and similar for h to re-write:

$$\frac{\partial}{\partial z} \tilde{E}_0(q_x, q_y, z) = \left[\frac{-ik}{2 \cos(\alpha_0)} \chi_0 - \frac{i2\pi}{\cos(\alpha_0)} q_{0,\perp} \right] \tilde{E}_0(q_x, q_y, z) - \frac{ik}{2 \cos(\alpha_0)} \mathcal{F}_\perp \{ \chi'_h(x,y,z) E_h(x,y,z) \} \quad (8)$$

where $q_{0,\perp} = \mathbf{q} \cdot \mathbf{k}_{0,\perp} / k$.

In cases where χ'_h is constant or depends only on z the problem can be solved analytically with Green's function methods. In the general case where χ_h varies as a function of all coordinates, the scattering term: $\mathcal{F}_\perp \{ \chi'_h(x,y,z) E_h(x,y,z) \}$ cannot be simplified and we have to use finite difference methods to solve the equations.

We note that in cases when both \mathbf{k}_0 and \mathbf{k}_h lie within the x-y plane, the 2D Fourier transforms may be replaced by 1D Fourier transforms along the x-direction.

We introduce a computational grid with axes parallel to the coordinate system. It has step sizes d_x , d_y and d_z and number of points, in each dimension, N_x , N_y and N_z . A point on the grid $P = (i_x d_x, i_y d_y, i_z d_z)$ can be indexed by the numbers i_x, i_y, i_z where $i_z = 0, 1, 2 \dots N_z - 1$ and so on.

In order to utilize discrete Fourier transform methods when solving these equations on a finite grid, we impose zero Dirichlet boundary conditions in the two transverse dimensions, x and y :

$$\begin{aligned} E_0(0,y,z) = E_0(L_x,y,z) = E_h(0,y,z) = E_h(L_x,y,z) = 0 \\ E_0(x,0,z) = E_0(x,L_y,z) = E_h(x,0,z) = E_h(x,L_y,z) = 0 \end{aligned} \quad (9)$$

These boundary conditions mean that the sample grid has to be large enough to fit the Bormann triangle extending from every point where the initial condition is non-zero. This means that if the initial condition is non-zero only on a domain Ω on the surface $z = 0$, then the direct projection of this domain along the directions of \mathbf{k}_0 and \mathbf{k}_h must lie within the sample grid. (see Fig 1)

This is fulfilled if the domain Ω is fully contained in the rectangle defined by:

$$\max(0, Lk_{0x}/k, Lk_{hx}/k) < x < \min(L_x, L_x + Lk_{0x}/k, L_x + Lk_{hx}/k) \quad (10)$$

$$\max(0, Lk_{0y}/k, Lk_{hy}/k) < y < \min(L_y, L_y + Lk_{0y}/k, L_y + Lk_{hy}/k) \quad (11)$$

which can always be made true for a finitely bounded initial condition if the computational grid is chosen sufficiently large. We use the initial conditions in z : $E_h(x,y,0) = 0$ and $E_0(x,y,0) = E_{\text{init}}(x,y)$. With these boundary conditions, the TTEs become a linear homogeneous initial value problem in z and the integration can be performed with an appropriate finite difference scheme.

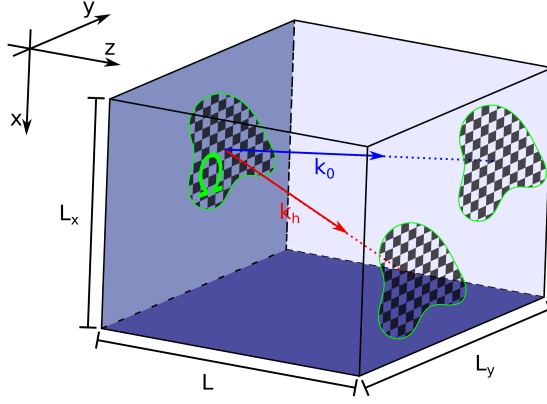


Figure 1. Scattering geometry inside the sample volume and the finite support of the initial condition.

3 FINITE DIFFERENCE SCHEMES

Collecting the discretized components of $\tilde{E}_0(\mathbf{q}_\perp, z)$ and $\tilde{E}_h(\mathbf{q}_\perp, z)$ into a single vector, \mathbf{E} , the equations (8) can be written on the form, $\frac{\partial}{\partial z}\mathbf{E} = \mathbf{A}\mathbf{E} + \mathbf{B}(z, \mathbf{E})$, where \mathbf{A} is a diagonal matrix containing the coefficients in the square brackets of equation (8) and \mathbf{B} contains the convolution terms. In this form, the system of equations can be solved by an exponential integrator, where the \mathbf{A} -term is handled exactly by an exponential function and the \mathbf{B} -term is handled by a finite difference scheme. Hochbruck and Ostermann (2010)

To test the convergence, we utilize two different exponential integrators. The archetypal exponential integrator based on the explicit Euler scheme is given by:

$$\mathbf{E}(z+h) = \exp(h\mathbf{A})\mathbf{E}(z) + h(h\mathbf{A})^{-1}(\exp(h\mathbf{A}) - 1)\mathbf{B}(z, \mathbf{E}(z)) \quad (12)$$

Higher order methods can be constructed in a systematic way. One such explicit second order method based on Heun's methods is given by the steps: Friedli (1978)

$$\begin{aligned} E_1^* &= \mathbf{E}(z) \\ b_1 &= \mathbf{B}(z_n, E_1^*) \\ E_2^* &= \phi_0 E_1^* + h\phi_1 b_1 \\ b_2 &= \mathbf{B}(z_n + h, E_2^*) \\ \mathbf{E}(z+h) &= \phi_0 E_1^* + \frac{h}{2}((2\phi_1 - \phi_2)b_1 + \phi_2 b_2) \end{aligned} \quad (13)$$

where the ϕ -functions are given by: $\phi_0 = \exp(h\mathbf{A})$ and $\phi_n = n(h\mathbf{A})^{-1}(\phi_{n-1} - 1)$.

The scheme based on Heun's method is chosen here because it only evaluates the \mathbf{B} function on the same regular intervals where the field is calculated, and therefore only needs the value of the scattering function on the same grid where the fields are evaluated.

For comparison with existing methods we also use a normal finite difference method based on a recent publication by Shabalin et al. (2017) using the half-step finite difference for the derivatives. A derivation of this method is given in Appendix A.

4 CONVERGENCE BEHAVIOUR OF EXPONENTIAL METHODS

We choose a symmetric geometry with the scattering vector aligned with the x -axis and scattering angle of $2\theta = 21^\circ$, which is typical for hard x-ray diffraction microscopy experiments. (see for example Poulsen

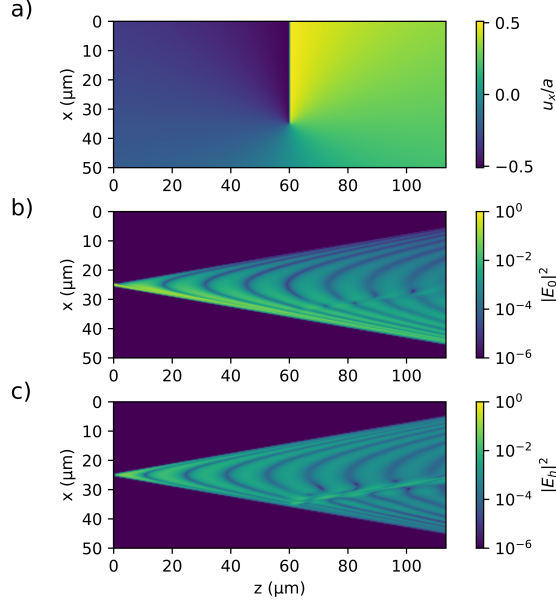


Figure 2. Plots of the sample and calculated fields used in the second convergence test. a) displacement field in units of the lattice constant, a . b) Transmitted field on a logarithmic scale, c) scattered field on a logarithmic scale.

et al. (2017)) We use a sample consisting of a perfect single crystal with a single edge dislocation with Burger's vector (100) close to the path of the direct beam. A plot of the displacement field as well as the amplitudes of the converged solution is shown in figure 2. The fields are simulated under low absorption and highly dynamical conditions.

We simulate only a single slice in the y -direction with the dimensions $50\mu\text{m} \times 115\mu\text{m}$ at a point $1\mu\text{m}$ from the dislocation core. The incident beam is a narrow Gaussian of width $\sigma = 0.2\mu\text{m}$.

In order to accommodate the comparison with existing methods, we utilize a grid with step sizes $\Delta z = h$ and $\Delta x = 2 \tan(\theta)h$ for the exponential methods and a grid with the same density of points for the normal finite difference method (see appendix A).

To check the convergence of the methods we calculate the fields on progressively finer grids. The first grid consisting of only 101×41 points. The error is calculated from the difference on the final slice compared to the solution found with the normal finite difference approach on a very fine grid of $10,241 \times 25,601$ steps evaluated on the points of the coarse grid on the exit surface where every grid coincides.

Figure 3 shows the convergence of the three integration methods that all show the expected convergence on a perfect sample a), but the traditional half-step method does not show the expected second order convergence with the edge dislocation sample b). The first order exponential Euler method suffers from an exponential instability and only gives a qualitatively correct result when impractically small step-sizes are utilized.

5 INCLUDING DISPERSION TERMS IN THE TTE'S

The method as we present it is a mixed real space - reciprocal space method and is conceptually similar to a FFT-based multi slice scheme used to propagate a wave-field through thick optical components. The value of FFT based methods in those situations is that the dispersion of the beam can easily be handled

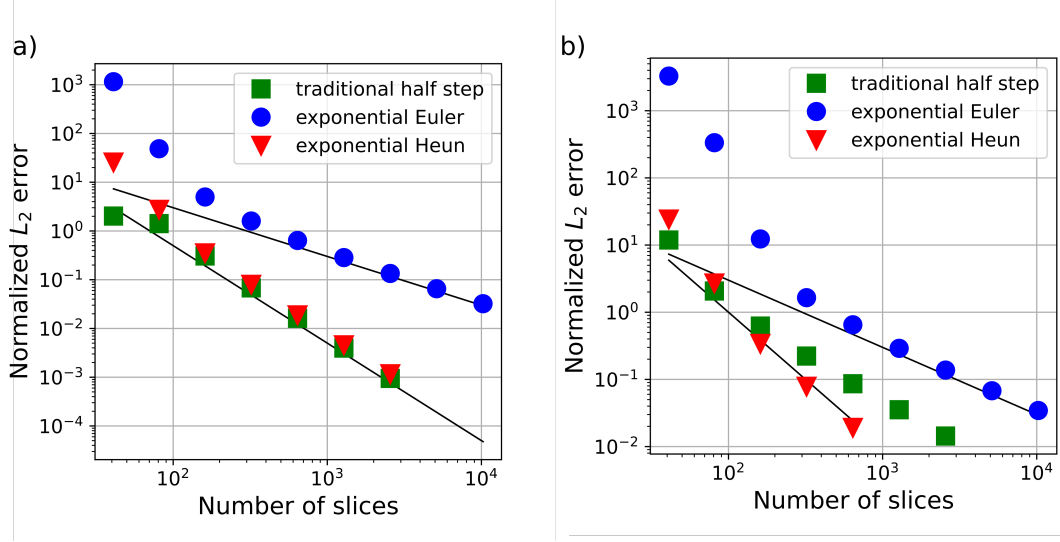


Figure 3. Convergence of the new exponential integrators and a traditional finite difference scheme. The black lines mark first- and second-order convergence respectively. All errors are calculated relative to the solution using the traditional half step method with 10,241 steps. We tested integration schemes on two different samples. One a) is a perfect crystal the other b) is the edge dislocation type sample shown in Fig. 2

in the paraxial approximation. Typically the dispersion terms are omitted in the TTEs, thus effectively making the projection approximation.

If the dispersion terms are kept, a different version of the TTEs can be written:

$$\begin{aligned} 2i\mathbf{k}_0 \cdot \nabla E_0(\mathbf{r}) &= k^2(\chi_0 E_0(\mathbf{r}) + \chi'_h(\mathbf{r}) E_h(\mathbf{r})) + \nabla^2 E_0(\mathbf{r}) \\ 2i\mathbf{k}_h \cdot \nabla E_h(\mathbf{r}) &= k^2(\chi_0 E_h(\mathbf{r}) + \chi'_h(\mathbf{r}) E_0(\mathbf{r})) + \nabla^2 E_h(\mathbf{r}) \end{aligned} \quad (14)$$

which handles dispersion of the incident and scattered beam inside the crystal. Pair of equations can be solved by the finite difference scheme presented here without any increase of computational complexity. (see Appendix B) We find that the approximation made by omitting the dispersion term is small in situations of practical interest but can be significant if the incident radiation contains very high-frequency components.

6 DISCUSSION

We have shown a finite difference capable of integrating the TTEs on an orthogonal grid with few restrictions on the choice of grid. We achieve this by implicitly utilizing Fourier interpolation at the level of the individual finite difference step. The method makes approximately the same error as the traditional half-step finite difference scheme.

The ability to freely choose the computational grid makes implementation of this approach easier, especially when it needs to be combined with other numerical modelling methods. For example if the the input for either the crystal micro structure or the incident field is given by a numerical simulation, or if the scattered fields should be propagated through image-forming optics.

The price to pay for this freedom to choose the grid, is that the method utilizes FFTs at each step and has to perform in total 4 2D Fourier transforms (1D in certain symmetric geometries) of the entire sample volume, which is expected to be a high computational cost compared to the existing methods.

our experience here, using un-optimized code, is that this increase amounts to about a factor of 4, which should be affordable in many cases.

REFERENCES

- Authier, A., Malgrange, C., and Tournarie, M. (1968). Etude théorique de la propagation des rayons X dans un cristal parfait ou légèrement déformé. *Acta Crystallographica Section A*, 24(1):126–136.
- Bremer, J. (1984). The two-wave X-ray field calculated by means of integral-equation methods. *Acta Crystallographica Section A*, 40(3):283–291.
- Epelboin, Y. (1981). A varying-step algorithm for the numerical integration of Takagi–Taupin equations. *Acta Crystallographica Section A*, 37(1):132–133.
- Friedli, A. (1978). Verallgemeinerte Runge-Kutta Verfahren zur Lösung steifer Differentialgleichungssysteme. In *Numerical treatment of differential equations (Proc. Conf., Math. Forschungsinst., Oberwolfach, 1976)*, pages 35–50. Lecture Notes in Math., Vol. 631.
- Hochbruck, M. and Ostermann, A. (2010). Exponential integrators. *Acta Numerica*, 19:209–286.
- Honkanen, A.-P., Ferrero, C., Guigay, J.-P., and Mocella, V. (2018). A finite-element approach to dynamical diffraction problems in reflection geometry. *Journal of Applied Crystallography*, 51(2):514–525.
- Kolosov, S. and Punegov, V. (2005). Numerical integration methods for the Takagi-Taupin equations for crystals of rectangular cross section. *CRYSTALLOGRAPHY REPORTS*, 50(3):357–362.
- Li, P., Maddali, S., Pateras, A., Calvo-Almazan, I., Hruszkewycz, S., Cha, W., Chamard, V., and Allain, M. (2020). General approaches for shear-correcting coordinate transformations in Bragg coherent diffraction imaging. Part II. *Journal of Applied Crystallography*, 53(2):404–418.
- Osterhoff, M. (2012). *Wave optical simulations of x-ray nano-focusing optics*, volume 009 of *Göttingen Series in x-ray Physics*. Universitaetsverlag Goettingen, Goettingen.
- Poulsen, H. F., Jakobsen, A. C., Simons, H., Ahl, S. R., Cook, P. K., and Detlefs, C. (2017). X-ray diffraction microscopy based on refractive optics. *Journal of Applied Crystallography*, 50(5):1441–1456.
- Shabalin, A. G., Yefanov, O. M., Nosik, V. L., Bushuev, V. A., and Vartanyants, I. A. (2017). Dynamical effects in bragg coherent x-ray diffraction imaging of finite crystals. *Phys. Rev. B*, 96:064111.
- Takagi, S. (1962). Dynamical theory of diffraction applicable to crystals with any kind of small distortion. *Acta Crystallographica*, 15(12):1311–1312.
- Takagi, S. (1969). A dynamical theory of diffraction for a distorted crystal. *Journal of the Physical Society of Japan*, 26(5):1239–1253.
- Taupin, D. (1967). Prévision de quelques images de dislocations par transmission des rayons X (cas de Laue symétrique). *Acta Crystallographica*, 23(1):25–35.
- Yan, H. and Li, L. (2014). X-ray dynamical diffraction from single crystals with arbitrary shape and strain field: A universal approach to modeling. *Phys. Rev. B*, 89:014104.

A TRADITIONAL FINITE DIFFERENCE SCHEME

For comparison with the exponential integrators presented in this paper, we also present calculations performed with the 2nd order implicit finite difference scheme based on central difference estimate for the derivatives, which is most usually applied for dynamical scattering calculations. The derivation here follows the one given by Shabalin et al. (2017) with small changes to the notation.

We limit our attention to a symmetric geometry defined by:

$$\mathbf{k}_0 = k(\sin(\theta), 0, \cos(\theta)) \quad \text{and} \quad \mathbf{k}_1 = k(-\sin(\theta), 0, \cos(\theta)) \quad (15)$$

Starting from equation (5) we introduce the coordinates:

$$\begin{bmatrix} s_0 \\ s_h \end{bmatrix} = \begin{bmatrix} \sin \theta & \cos \theta \\ -\sin \theta & \cos \theta \end{bmatrix} \begin{bmatrix} x \\ z \end{bmatrix} \quad (16)$$

and arrive at a well-known form of the Takagi-Taupin equations: (suppressing the y-dependence)

$$\begin{aligned} \frac{\partial E_0(s_0, s_h)}{\partial s_0} &= \frac{k}{2i} (\chi_0 E_0(s_0, s_h) + \chi'_h(s_0, s_h) E_h(s_0, s_h)) \\ \frac{\partial E_h(s_0, s_h)}{\partial s_h} &= \frac{k}{2i} (\chi_0 E_h(s_0, s_h) + \chi'_h(s_0, s_h) E_0(s_0, s_h)) \end{aligned} \quad (17)$$

To avoid truncation errors due the complex rotation caused by the χ_0 terms, we introduce the scaled fields $E_0' = \exp(\chi_0 \frac{ik}{2} s_0)$ and $E_h' = \exp(\chi_0 \frac{ik}{2} s_h)$. Plugging in and simplifying some terms gives:

$$\begin{aligned} \frac{\partial E_0'(s_0, s_h)}{\partial s_0} &= \frac{k}{2i} \exp\left(\chi_0 \frac{ik}{2} (s_0 - s_h)\right) \chi'_h(s_0, s_h) E_h'(s_0, s_h) \\ \frac{\partial E_h'(s_0, s_h)}{\partial s_h} &= \frac{k}{2i} \exp\left(\chi_0 \frac{ik}{2} (s_h - s_0)\right) \chi'_h(s_0, s_h) E_0'(s_0, s_h) \end{aligned} \quad (18)$$

We now introduce a rectangular grid in the original (x, y) -coordinates with step-size h in the z direction and $h \tan(\theta)$ in the x -direction. With this choice of grid a subset consisting of every second grid point constitutes a sheared grid aligned with the s_0 and s_h directions with both step sizes equal to $p = h(1 + \tan(\theta)^2)^{1/2}$. This allows us to calculate the fields using the finite difference methods and the exponential integrators on grids with the same density of grid points and that coincide on every second plane. We therefore have to choose a grid with an odd number of grid points in the x -direction so that we can compare the result on the final slice. (see figure 4)

We denote the discretized envelope fields by $E'(x_j, z_i) = E^{i,j}$. The recurrence relation is obtained by the centered first order approximation for the derivatives and a similar centered approximation for the right hand sides in equation (18) to arrive at the equations:

$$\begin{aligned} \frac{E_0^{i,j} - E_0^{i-1,j-1}}{p} &= \frac{k}{2i} B \frac{E_h^{i,j} + E_h^{i-1,j-1}}{2} \\ \frac{E_h^{i,j} - E_h^{i-1,j+1}}{p} &= \frac{k}{2i} D \frac{E_0^{i,j} + E_0^{i-1,j+1}}{2} \end{aligned} \quad (19)$$

where

$$B = \exp\left(\chi_0 \frac{ik}{2} (s_0^{i,j} - s_h^{i,j} - p/2)\right) \chi'_h\left(s_0^{i,j} - p/2, s_h^{i,j}\right)$$

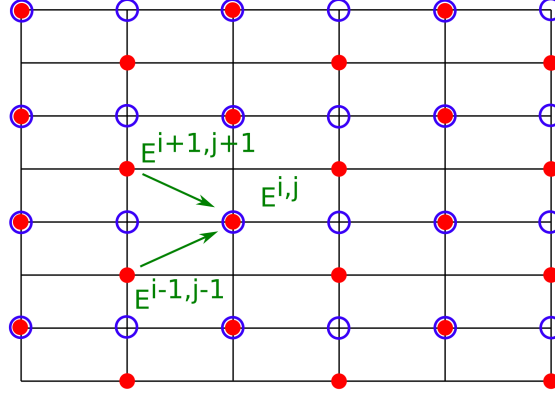


Figure 4. Computational grids used for the traditional half-step approach marked with red dots and for the exponential integrators marked with blue circles. The recurrence relation for the half-step method is drawn with green arrows.

and

$$D = \exp\left(\chi_0 \frac{ik}{2}(s_h^{i,j} - s_0^{i,j} - p/2)\right) \chi_h(s_0^{i,j}, s_h^{i,j} - p/2)$$

introducing the constant $A = \frac{4i}{kp}$ we can finally write:

$$\begin{aligned} E_0^{i,j} &= E_0^{i-1,j-1} + B/AE_h^{i,j} + B/AE_h^{i-1,j-1} \\ E_h^{i,j} &= E_h^{i-1,j+1} + D/AE_0^{i,j} + D/AE_0^{i-1,j+1} \end{aligned} \quad (20)$$

which are the implicit recurrence relations used in the calculations. Furthermore we need the boundary conditions, that the fields are both zero at the top and bottom surfaces: $E_{0/h}^{i,0} = E_{0/h}^{i,N_x-1} = 0$

B OFF-AXIS PARAXIAL OPTICS

The paraxial approximation deals with the laplacian term by assuming that the complex envelope of the beam is slowly varying in the direction of propagation and therefore discarding the z -derivative term. There is one small complication with doing the paraxial approximation in our case: the coordinate system is not fixed to the direction of beam propagation as we have two beams propagating in different directions.

For simplicity of the notation here we assume that the scattering plane coincides with the x - z plane and define the angles, α_0 and α_h through:

$$\mathbf{k}_0 = (\sin \alpha_0, 0, \sin \alpha_0) \quad \text{and} \quad \mathbf{k}_h = (\sin \alpha_h, 0, \sin \alpha_h) \quad (21)$$

but generalization to other geometries is straight forward. We introduce a coordinate-system rotated onto one of the two beams:

$$(x', y', z') = R_\alpha \mathbf{r} = (\cos(\alpha)x - \sin(\alpha)z, y, \cos(\alpha)z + \sin(\alpha)x) \quad (22)$$

In the new coordinates we discard the z derivative term of the laplacian and re-express it in the old

coordinates:

$$\begin{aligned}\nabla^2 &\approx \frac{\partial^2}{\partial x^2} + \frac{\partial^2}{\partial y^2} = \cos^2(\alpha) \frac{\partial^2}{\partial x^2} - 2 \sin(\alpha) \cos(\alpha) \frac{\partial^2}{\partial x \partial z} + \sin^2(\alpha) \frac{\partial^2}{\partial z^2} + \frac{\partial^2}{\partial y^2} \\ \frac{\partial^2}{\partial z^2} &= \cos^2(\alpha) \frac{\partial^2}{\partial x^2} - 2 \sin(\alpha) \cos(\alpha) \frac{\partial^2}{\partial x \partial z} + \sin^2(\alpha) \frac{\partial^2}{\partial x^2} \approx 0\end{aligned}\quad (23)$$

Using these two equations to eliminate the second order derivative in z gives:

$$\nabla^2 \approx (1 - \tan^2(\alpha)) \frac{\partial^2}{\partial x^2} + 2 \tan(\alpha) \frac{\partial^2}{\partial x \partial z} + \frac{\partial^2}{\partial y^2}\quad (24)$$

Using this approximation for the laplacian terms in Eq. (14) yields the modified version of Eq. (8) given by:

$$\begin{aligned}\frac{\partial}{\partial z} \tilde{E}_0 &= \frac{-i}{2(\cos(\alpha_0)k + \tan(\alpha_0)q_x)} [k^2 \chi_0 + 2 \sin(\alpha_0) v_x k + q_y^2 + (1 - \tan^2(\alpha_0)) q_x^2] \tilde{E}_0 \\ &\quad - \frac{ik^2}{2(\cos(\alpha_0)k - \tan(\alpha_0)q_x)} \mathcal{F}_\perp \{ \chi_h \mathcal{F}_\perp^{-1} \{ \tilde{E}_h \} \} \\ \frac{\partial}{\partial z} \tilde{E}_h &= \frac{-i}{2(\cos(\alpha_h)k + \tan(\alpha_h)q_x)} [k^2 \chi_0 + 2 \sin(\alpha_h) q_x k + q_y^2 + (1 - \tan^2(\alpha_h)) q_x^2] \tilde{E}_h \\ &\quad - \frac{ik^2}{2(\cos(\alpha_h)k - \tan(\alpha_h)q_x)} \mathcal{F}_\perp \{ \chi_h \mathcal{F}_\perp^{-1} \{ \tilde{E}_0 \} \}\end{aligned}\quad (25)$$

This equation defines new expressions for the coefficients of the A-matrix and pre-factors of the B-function but adds no computational complexity to the exponential integration beyond that. Figure 5 shows that the off-axis paraxial propagator defined by equation (25) (omitting the scattering terms) gives the correct result for a paraxial Gaussian beam.

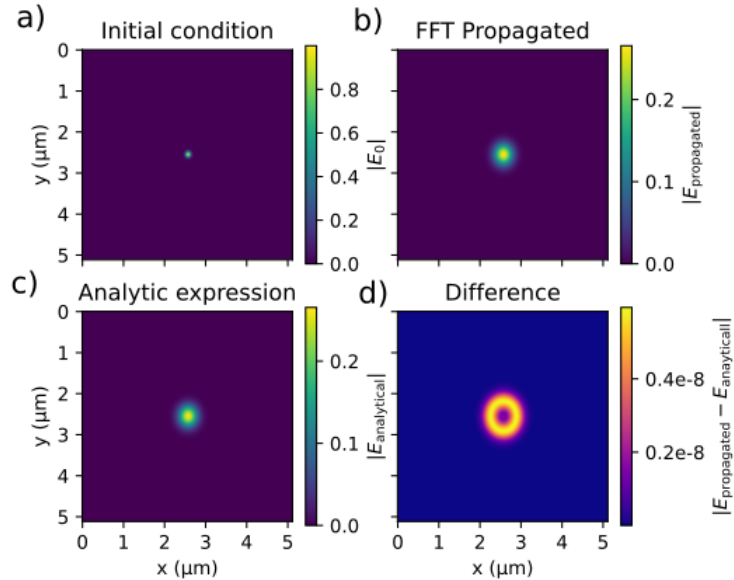


Figure 5. Off-axis paraxial optics propagation of a circular Gaussian beam at an angle $\alpha = 30^\circ$ using the 1-beam version of Eq. (25) and omitting the sin term, which interpolates the beam. a) Beam at $z=0$. b) FFT-propagated beam at $z = 1$ mm. c) Analytic expression of beam intensity at $z = 1$ mm d) Difference between FFT-propagated and analytical result. The relative error compared to the analytical expression is about 10^{-8} .